OECD/MCCI-2008-TR06

OECD MCCI Project
Small-Scale Water Ingression and Crust Strength Tests (SSWICS)
SSWICS-12 Design Report

Rev. 1 - FINAL

March, 2009

by:

S. Lomperski, A. Ramirez, M. T. Farmer, D. Kilsdonk, R. Aeschlimann

Nuclear Engineering Division
Argonne National Laboratory
9700 S. Cass Avenue
Argonne, IL 60439
USA

Table of Contents

1. Introduction.....1

2. System Description.....2

2.1 General.....2

2.2 Melt Partition.....2

2.3 Injection Supply System.....7

2.4 Injection Nozzles.....9

3. Data Acquisition and Control Systems.....12

3.1 Instrumentation.....12

3.2 General.....13

4. Test Parameters.....14

5. References.....17

Appendix A: Thermite and Nozzle Scoping Tests.....18

1. Introduction

The Melt Attack and Coolability Experiments (MACE) program at Argonne National Laboratory addressed the issue of the ability of water to cool and thermally stabilize a molten core/concrete interaction (MCCI) when the reactants are flooded from above. These experiments provided unique, and for the most part repeatable, indications of heat transfer mechanisms that could provide long term debris cooling. The tests provided data regarding the nature of corium interactions with concrete, the heat transfer rates from the melt to the overlying water pool, and the role of noncondensable gases in the mixing processes that contribute to melt quenching. However, due to the integral nature of the tests, several questions regarding the crust freezing behavior could not be adequately resolved. These questions include:

- To what extent does water ingression into the crust increase the melt quench rate above the conduction-limited rate and how is this affected by melt composition and system pressure?
- What is the fracture strength of the corium crust when subjected to a particular thermal-mechanical load and how does it depend upon the melt composition?

A series of separate-effects experiments was carried out during the MCCI-1 program to address these issues. A test apparatus denoted SSWICS (Small Scale Water Ingression and Crust Strength) was constructed and used to quench ϕ30 x 15 cm deep melts at atmospheric pressure and also at 4 bar. The data indicated that the rate of cooling associated with water ingression, which occurs via cracks induced by thermal stresses, decreases with increasing melt concrete content. In addition, the cooling rate was shown to be insensitive to concrete type and system pressure. Companion experiments determined the strength of the ingots produced by these quench tests and it was found that the extensive cracking within the corium made the material structurally weak and that strength is essentially independent of corium composition over the tested composition range.

The SSWICS tests for the MCCI-1 program were generic in nature and were intended to validate water ingression models that predict ex-vessel corium cooling rates. Data was also generated to validate structural models used to predict the strength of corium crusts. The test described in this report, SSWICS-12, differs from those of the previous program in that it is intended to demonstrate the performance characteristics of a particular type of engineered corium cooling system. The system is designed to inject water into the corium from below to enhance the cooling rate far beyond that achievable by top flooding alone.

SSWICS-12 will be similar in many respects to the preceding tests, e.g., fully oxidized melt with concrete constituents, 30 cm melt diameter, inert basemat, quench at 1 bar, and condensation of steam with collection of the condensate to measure gross cooling rate. The major departure from previous tests is the addition of water injection nozzles cast within the basemat. Each injection line will have its own water supply and flow rate sensor. The melt will be partitioned into quadrants using metal plates to create, in effect, four independent and simultaneous injection tests. Each nozzle is to have a different driving head. The purpose of this experiment is to determine the following:

- the minimum driving head required to ensure water injection into the melt
- the water flow rate to each nozzle
- the cooling rate of each melt quadrant
- the effect of water injection on crust morphology

The melt depth will be 30 cm (versus 15 cm for all previous tests) so that it is closer to the 20-30 cm depth expected in a plant. The remainder of this report describes the test apparatus, instrumentation, test procedure, and data reduction.

2. System Description

2.1 General

The SSWICS reaction vessel (RV) has been designed to hold at least 100 kg of melt at an initial temperature of 2500°C. The RV lower plenum consists of a 67.3 cm long, 45.7 cm outer diameter carbon steel pipe (Fig. 2.1). The pipe is insulated from the melt by a 6.4 cm thick annulus of cast MgO that is denoted the "liner". The selected pipe and insulation dimensions result in a melt diameter of 30 cm and a surface area of 707 cm^2. The melt depth for a typical corium charge of 75 kg is about 15 cm. The RV lower flange is insulated with a 6.4 cm thick slab of cast MgO (the "basemat") that spans the entire inner diameter of the pipe. The basemat and liner form the crucible that holds the corium.

The RV upper plenum consists of a second section of pipe with a stainless steel protective liner. Three 10 cm pipes welded near the top of the vessel provide 1) a vent line for the initial surge of hot noncondensable gases generated by the thermite reaction, 2) a pressure relief line with a rupture disk (7.7 bar at 100°C), and 3) an instrument flange for the absolute pressure transmitter that measures the reaction vessel pressure. A baffle is mounted below the upper flange prevents water droplets from being carried up towards the condenser, which would adversely affect the heat flux measurement. A fourth 10 cm pipe welded to the top flange provides an outlet to carry steam from the quenching melt to four cooling coils. The water-cooled coils condense the steam, which is collected within a 200 cm high, 20 cm diameter condensate tank (CT). Figure 2.2 provides a detailed view of the lower plenum and basemat while Fig. 2.3 gives an overview of the entire SSWICS melt-quench facility.

2.2 Melt Partition

The corium is to be divided into quadrants by thin plates. Because of the high initial melt temperature, only refractory materials are considered for plate construction. Since the test section diameter is only 30 cm, there is little room for cast MgO plates, which would be rugged but rather thick. Other types of ceramics may be cast as thin plates, but they would lack an acceptable level of thermal shock resistance. Refractory metals are deemed to be the most suitable material for the difficult task of partitioning a 2000°C melt. Tungsten and molybdenum are the two metals that have proven resistant to corium corrosion and are considered the only realistic candidates for the partition material. Molybdenum is easier to machine than tungsten, but we choose to select the partition material based on high temperature mechanical strength. Figure 2.4 shows the measured tensile strength of tungsten and molybdenum at high temperatures. At 2000°C, the strength of molybdenum is ~2 MPa and that of tungsten is ~5 MPa. For comparison, the room temperature yield strength of stainless steel is ~290 MPa. Since the strength of tungsten at 2000°C is twice that of molybdenum, tungsten is the recommended partition material.

The partition will be subjected to dynamic loads during the quench phase of the test as the water will vaporize almost immediately upon injection into the melt. There are likely to be asymmetries among partitions in water flow and vaporization rates that will generate lateral loads on the partition. In the extreme case, vapor explosions could occur and generate significant loads having the potential to rupture the partition. Still, the melt is quite dense and lateral forces that could bend the plate and displace melt in a neighboring partition might instead be redirected upwards where there is no mechanical restraint. From this it is evident that uncertainty in the partition loading is large and that it precludes the establishment of a firm design basis for the required partition strength. In short, it is not clear how strong the partition must be to ensure integrity of the four melt regions.

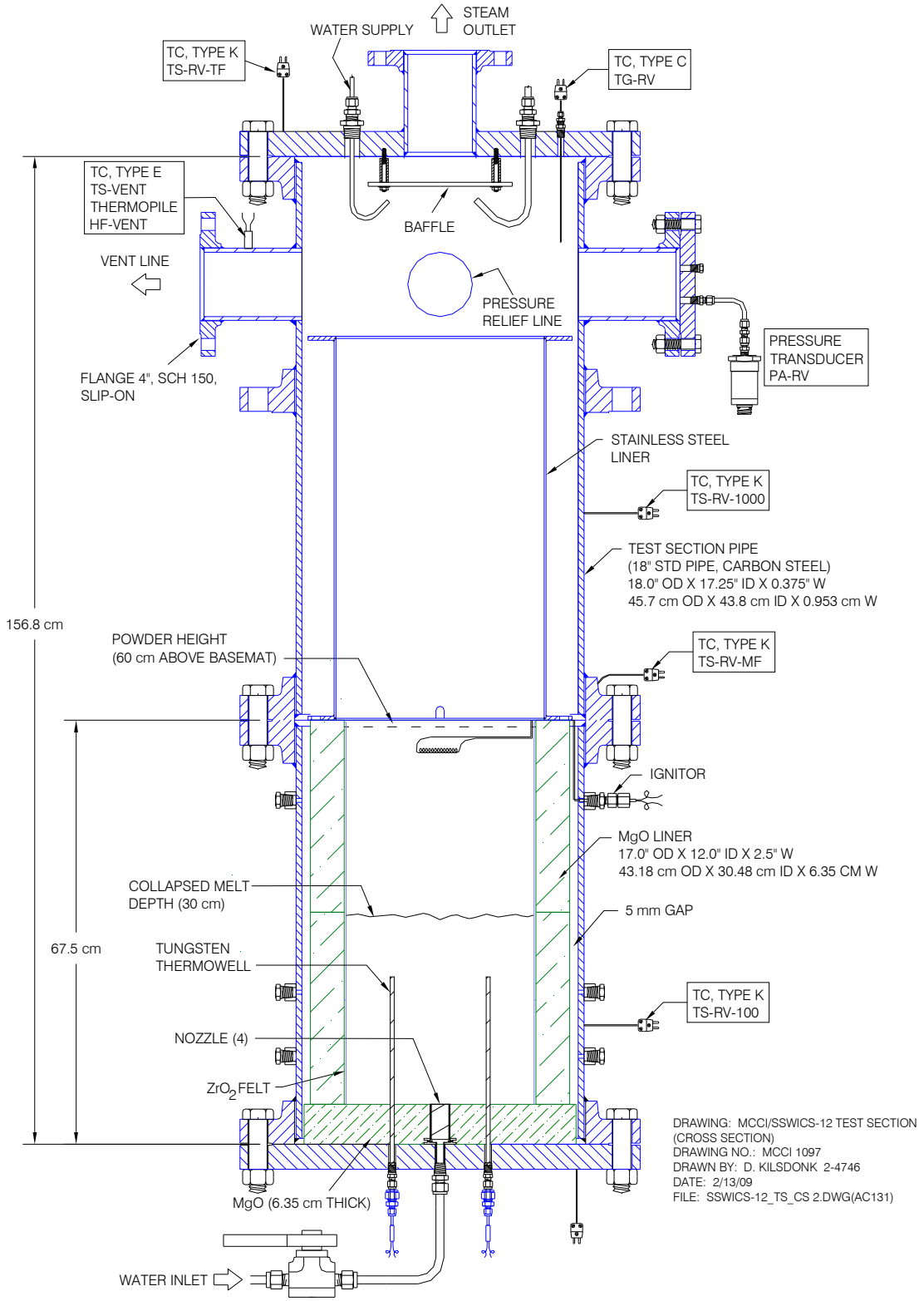

Figure 2.1. Side view of reaction vessel.

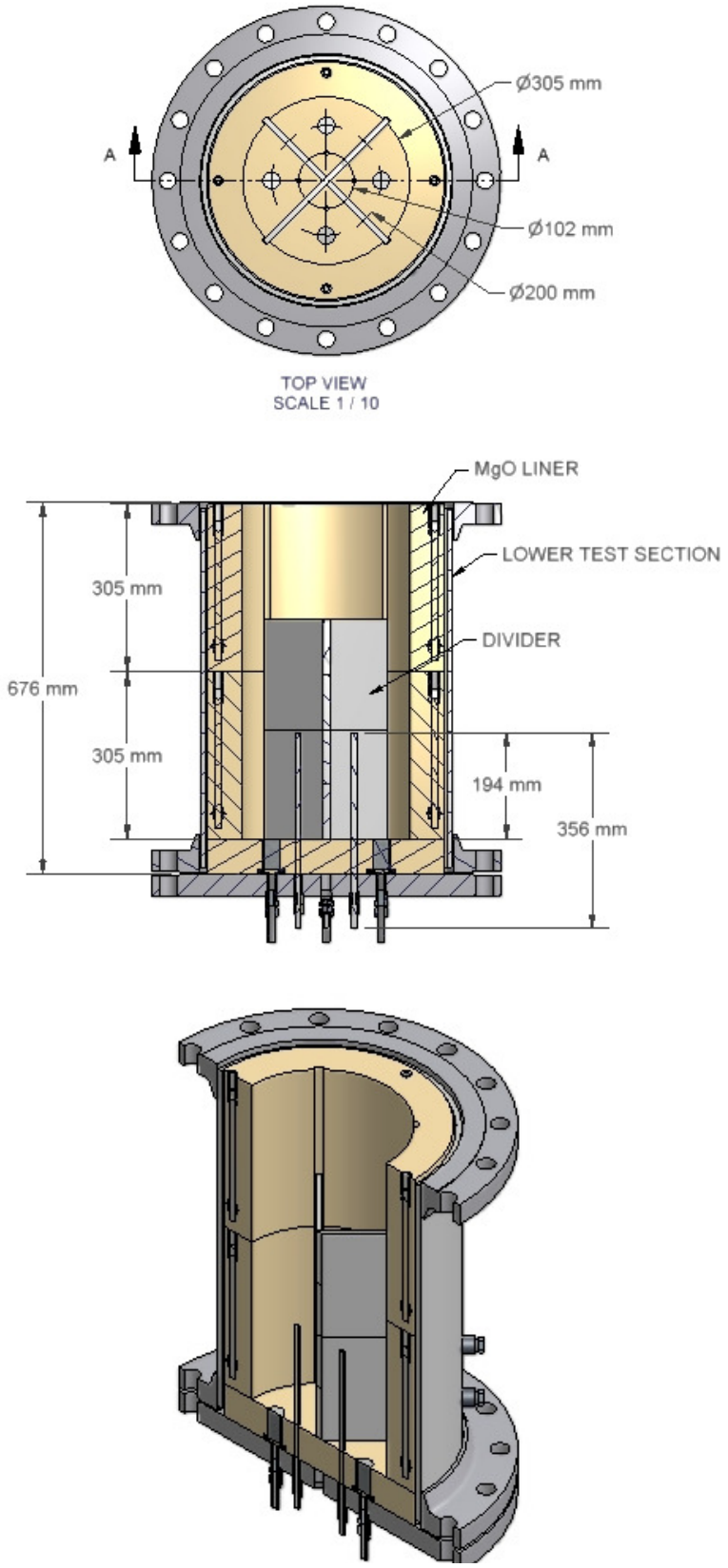

Figure 2.2. Lower plenum and basemat detail.

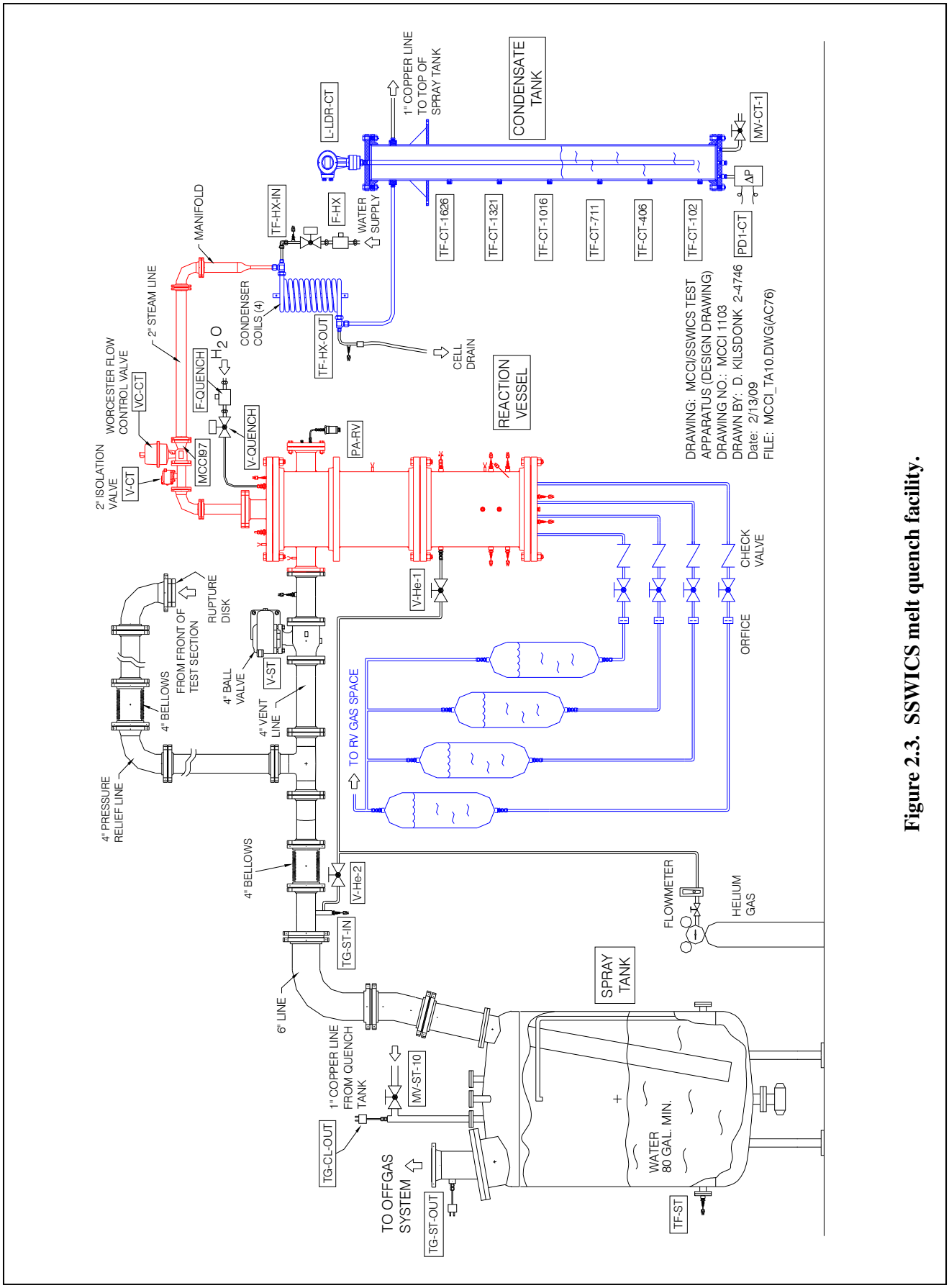

Figure 2.3. SSWICS melt quench facility.

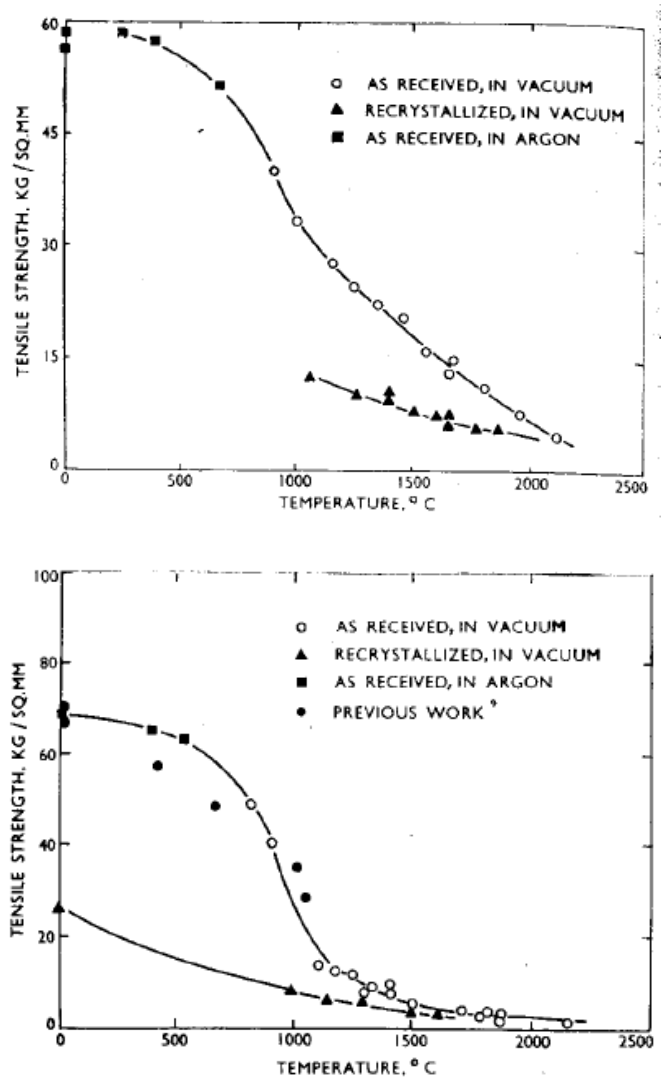

Figure 2.4. Tensile strength of tungsten (top) and molybdenum (bottom) [B. Mordike, J. Institute of Metals, vol. 88 1959-60].

The partitions are to be made of 10 mm thick tungsten plates with a machined slot so that one fits over the other in an interlocking cruciform (Fig. 2.5). The partition is supported by 20 mm deep grooves in the liner to discourage shifting under lateral loads. The partition consists of two stacked sections, each with a height of 20 cm, creating a 40 cm high wall within the melt.

We have no design basis criteria to judge the adequacy of the partition strength and indeed it would be difficult to assess its strength given the complex, slotted cruciform geometry. Alternatively, it may be useful to consider some simple geometries to obtain a sense of the strength of the partition at high temperature. The compartments formed by the partition are wedge-shaped, ~15 cm on three sides and 20 cm high. Consider a 15 cm sphere made of 10 mm thick tungsten at 2000°C. The sphere wall would begin to yield at a pressure of ~13 bar. Alternatively, a 15 x 20 x 1 cm thick plate, simply supported on three sides and free on one short side (the top of the partition), would yield under a uniform pressure of ~0.3 bar. These examples suggest that the partition is capable of bearing a significant load even when seriously weakened at the peak corium temperature. Thicker plates are available, but they would displace more of the melt volume and are more expensive. For example, the 10 mm plates reduce the melt surface area by 8% and cost (all four) ~$10k. The partition strength could be doubled with 20 mm plates, but both the area reduction and cost would likewise be doubled.

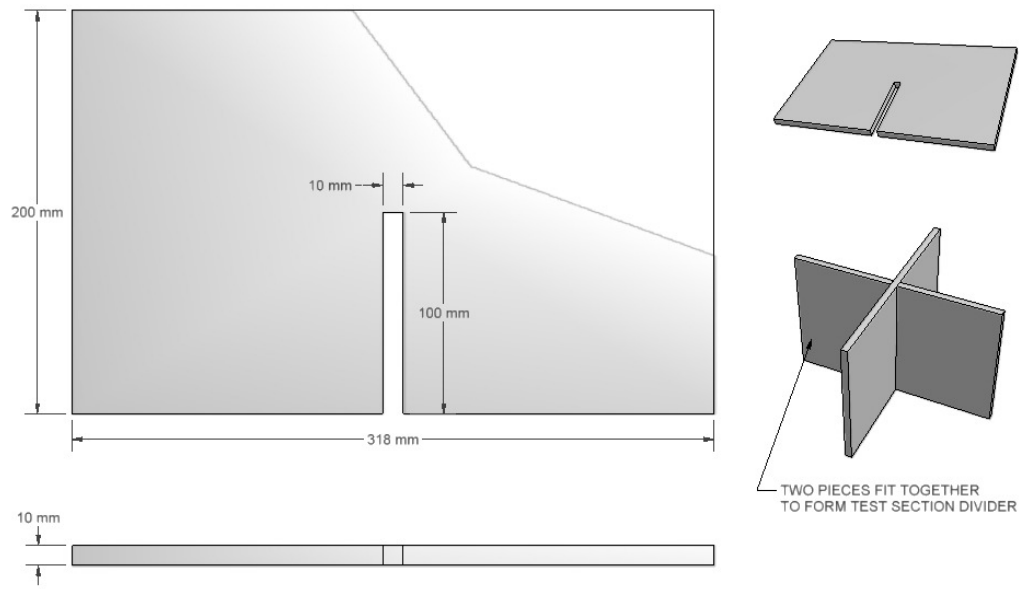

Figure 2.5. Construction detail for tungsten partition.

The tungsten insert not only displaces melt volume, but also serves as an undesired heat sink. As noted in Section 4, the proposed thermite for this test has been reformulated to increase the reaction temperature from the usual ~2000°C to 2100 ºC to help ensure that the nozzles are open for flow at the beginning of the test. The tungsten partitions will absorb energy from the thermite and depress the initial melt temperature. A thermal equilibrium calculation[1] indicates that the 10 mm plates will depress the initial equilibrium temperature ~75 ºC to ~2020 ºC. Thicker plates will further depress the equilibrium temperature. The reaction temperature cannot, unfortunately be increased to compensate for the heat sink because 2100°C is the practical limit for this melt composition.

2.3 Injection Supply System

Four 36-liter tanks provide independent reservoirs to supply the nozzles with water. The nozzles are gravity fed and so the driving pressure for injection is set by the elevation difference between the nozzle and the tank water level (Fig. 2.5). A check valve in each line prevents back flow up into the tank. There are also isolation valves in each line that will be opened when the RV preheat phase of the test begins.

The tanks are positioned at different levels to generate the desired range of driving pressures. A pressure equalization line links the RV gas space to the gas spaces of all four tanks, ensuring that the driving head for the nozzles is set only by the nozzle/tank elevation difference. This is necessary because the RV pressure spikes for a short period following initial water injection. If the reservoirs are not at the absolute pressure of the RV, the initial pressure spike will halt water injection, causing steam production and RV pressure to drop, which in turn permits continued water injection. It is likely that the system would oscillate during the early period of the test. Connecting the gas spaces of the reservoirs with that of the RV should prevent such oscillations.

[1] The assumed density, specific heat, and initial temperature of the tungsten cruciform are 19,250 kg/m^3, 134 J/kg-ºC, and 100 ºC, respectively. The corresponding assumptions for the corium are 6000 kg/m^3, 700 J/kg-ºC, and 2100 ºC, respectively.

Figure 2.6 shows the positioning of the tanks, which are set to provide initial net driving heads of 0.05, 0.1, 0.15, and 0.2 bar. The net driving head ΔP is defined here as the head remaining after subtracting the hydrostatic head associated with the melt:

$$\Delta P = \rho_l g L - \rho g h \big|_{corium}$$

where h is the height of the corium, 30 cm for this test, L is the distance from the bottom of the corium pool to the tank water surface, and ρ_l and ρ are the coolant and corium densities, respectively. The head associated with the corium was calculated to be 0.18 bar by assuming a density of 6000 kg/m^3. Assuming a water head of 10 meters/ bar, the tanks are positioned so that the water surfaces are 2.3, 2.8, 3.3, and 3.8 meters above the bottom of the corium pool.

In the interest of simplicity, no system is used to replenish the tanks during the test to maintain water level and so the driving head falls as water is injected into the melt. The drop in water level can be made small by using large-diameter tanks, but they serve as pressure vessels and so there is a strong incentive to

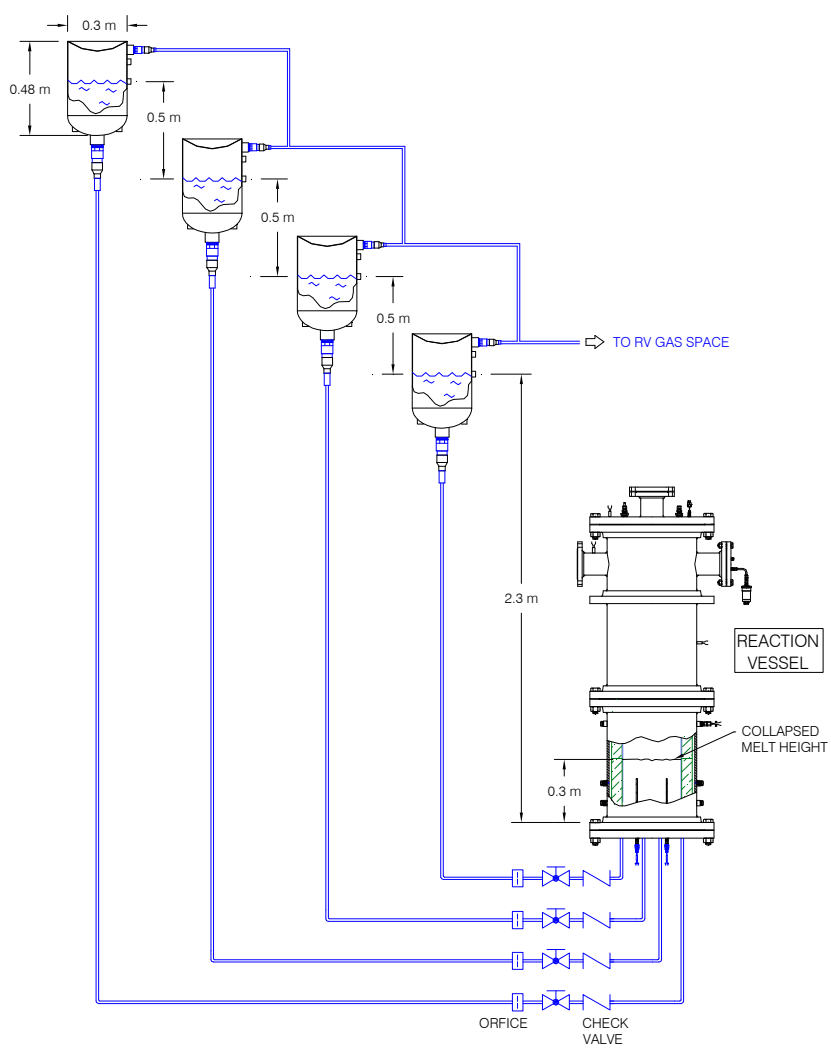

Figure 2.6. Water injection system geometry (drawn to scale).

minimize their size. Initial water inventory for each tank will be 20 liters, which was chosen by noting that approximately 30 liters of water is collected by the condensate tank during a typical 75 kg test. Since this test will involve 136 kg of corium and a higher than normal initial temperature, it is expected that about 60 liters of water will be boiled off while quenching the melt. All 80 liters from the four tanks will be injected into the RV since there are no remotely operated valves available to halt the gravity fed flow. Note that though extra water is injected to ensure that the melt remains covered during the entire course of the test, it is of interest to minimize excess water since the coolant will be at room temperature rather than near saturation as in recent tests. Test data is easier to interpret when saturated rather than subcooled water is injected.

During the early stage of the experiment, it is likely that water will be completely vaporized as it is injected into the melt. It is therefore necessary to limit the injection flow rate so that the condensing system is not overwhelmed. The condensing system has a capacity of approximately 0.08 kg/s. The flow limit is to be set at 50% this capacity. At this maximum flow of 0.01 kg/s to each partition, complete vaporization would dissipate 90 kW, or 1.3 MW/m^2.

Nozzle permeability is high enough that a restriction must be put in the injection line to prevent the flow rate from exceeding 0.01 kg/s. Appendix A describes scoping tests used to confirm this fact. Each line has an orifice sized to allow 0.01 kg/s at the initial fill level, which would empty the tanks in ½ hour if this maximum rate could be maintained. The injection rate will, however, decline with driving head and so the injection period will be longer. This is noted to emphasize that the water injection phase of the test will be much longer than that of previous SSWICS tests, which generally dispense with water injection in less than five minutes.

2.4 Injection Nozzles

The design for the concrete nozzles is shown in Fig. 2.7. Four nozzles are cast within the basemat and positioned so that they are roughly equidistant from the liner and neighboring partitions. The top of each nozzle is flush with the basemat surface and each is filled with porous concrete to provide a path for water flow up into the melt while preventing melt flow downward into the nozzle. The porous concrete filled nozzle is of interest because it mimics a proposed engineered corium cooling system. This separate effect test offers the opportunity to determine the behavior of the nozzle with prototypical corium.

A 0.05 mm-thick stainless steel diaphragm is welded over the top of each nozzle to serve as a temporary seal. The role of the diaphragm is to prevent water flow from the feed line up into the thermite during the vessel preheat phase of the experiment. Soon after the preheat phase begins, the isolation valves on the injection line will be opened. The diaphragms prevent water flow through the nozzles until thermite ignition melts the diaphragm. The diaphragms are expected to melt quickly since the initial temperature of the melt will be ~2100°C while the melting point of stainless steel is ~1400°C. A scoping test with 1.5 kg of thermite and a nozzle prototype confirmed that the diaphragm melts away shortly after thermite ignition.

The materials composition of the porous concrete, provided by FZK [1], is shown in Table 2.1. The ingredients are mixed together in a small pail until a homogeneous mixture is obtained and the material is poured into a steel tube that forms the outer shell of the nozzle.

Table 2.1. Material composition for porous concrete.

Concrete composition	**Wt %**
Gravel 2 – 4 mm	75
Mortar	25
Mortar composition	
Sand 0 – 1.6 mm	51.7
SiO_2 powder 0.0025 – 0.125 mm	5.9
Cement	27.0
Water	15.4

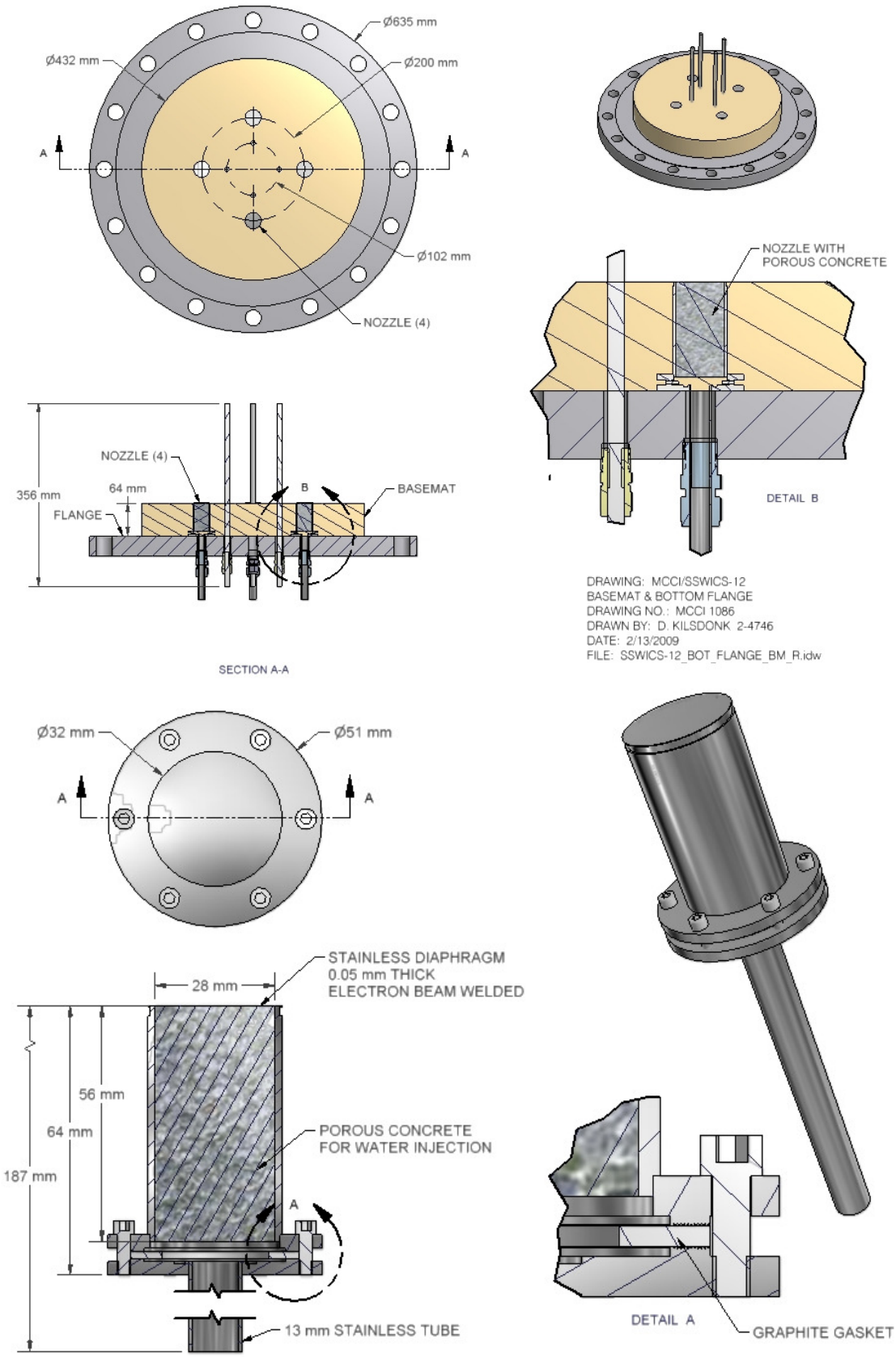

Figure 2.7 Nozzle layout on basemat (top) and nozzle detail (bottom).

3. Data Acquisition and Control Systems

3.1 Instrumentation

This test is intended to determine the efficacy of a particular engineered melt cooling concept. The directive to test a partitioned melt with separate injectors is, in effect, an instruction to combine four quench experiments into one. The instrumentation must therefore provide data sufficient to determine the boundary conditions and cooling behavior of individual partitions. The flow rate and driving pressure of each nozzle will be measured along with melt temperatures. The condensate collection and measurement system used in past tests to determine the steaming rate will also be used in this test, but it cannot provide the cooling rate of any particular partition. It will instead provide the gross melt cooling rate. Only indirect indications of individual partition cooling rates, obtained through measurements of melt temperature and water flow rate into each quadrant, are available for this test.

Since the cooling rate of each partition is of such importance and only thermocouples within the melt are able to provide germane data, more melt thermocouples will be used for this test than previous tests. Figure 3.1 shows the thermocouple layout in the basemat and the liner. Each partition is allotted a 5-junction C-type thermocouples in tungsten thermowells. The thermocouples are spaced every 51 mm so that the uppermost thermocouple is 190 mm above the basemat surface. The tungsten thermowells are 9.5 mm diameter, which is the same size used in CCI tests but larger than that used in previous SSWICS tests (6 mm). Though thermowell size should be minimized to limit fin cooling effects, the thermowells for this test are too long to fabricate in a diameter less than 9.5 mm.

Omitted from this test are the MgO liner thermocouples used in previous tests to detect water bypass around the melt at the melt/liner interface. These measurements are irrelevant here as water injection is expected to create widespread melt porosity that should indeed allow liquid flow across the melt/liner interface. Thus there is no notion here that water could go "around" the melt, as it might have during previous water ingression tests, distorting the predominantly one-dimensional character of the quench front.

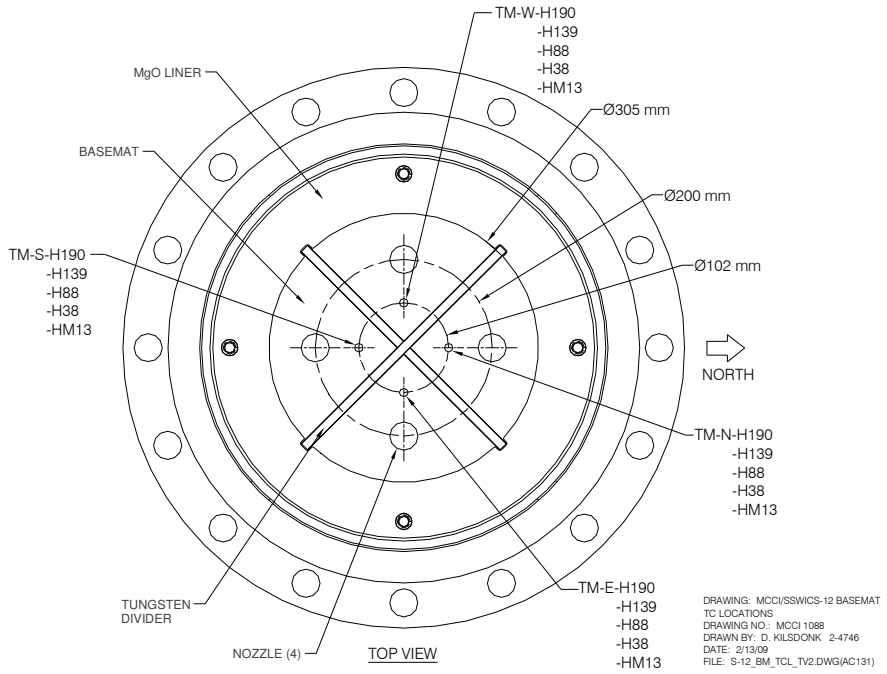

Figure 3.1. Melt thermocouple locations.

The nomenclature used to identify thermocouples is as follows: TM (temperature within the corium melt), TF (fluid temperature), TG (gas space temperature), TS (structure temperature), H# (height above the bottom of the melt, in mm, and N, S, E, W representing the cardinal points. The partition is to be situated so that the "wedges" face towards the cardinal points. For example, TM-N-H190 is the melt thermocouple in the north facing wedge, 190 mm above the bottom of the melt. An instrument list is provided in Tables 3.1.

3.2 General

All data acquisition and process control tasks are managed by a PC executing LabVIEW 8.2 under Windows XP. Sensor output terminals are connected to model HP E1345A 16-channel multiplexers and the signals are digitized by an HP E1326B 5 ½ digit multimeter located within the test cell (Fig. 3.2). Signal noise is reduced by integration over a single power line cycle (16.7 ms). The digitized sensor readings are routed from the test cell to the PC in the control room via two HP-IB extenders. The extenders allow the ASCII data from the HP to be sent through the cell wall over a BNC cable. The extender within the control room then communicates with a GPIB card within the PC. This configuration also permits remote control of the multimeter through LabVIEW. The power line cycle integration results in a minimum (theoretical) time of 0.75 s to scan the channel list (16.7 ms * 45 channels). In practice, however, the acquisition of a single scan is at a frequency of approximately 0.5 Hz.

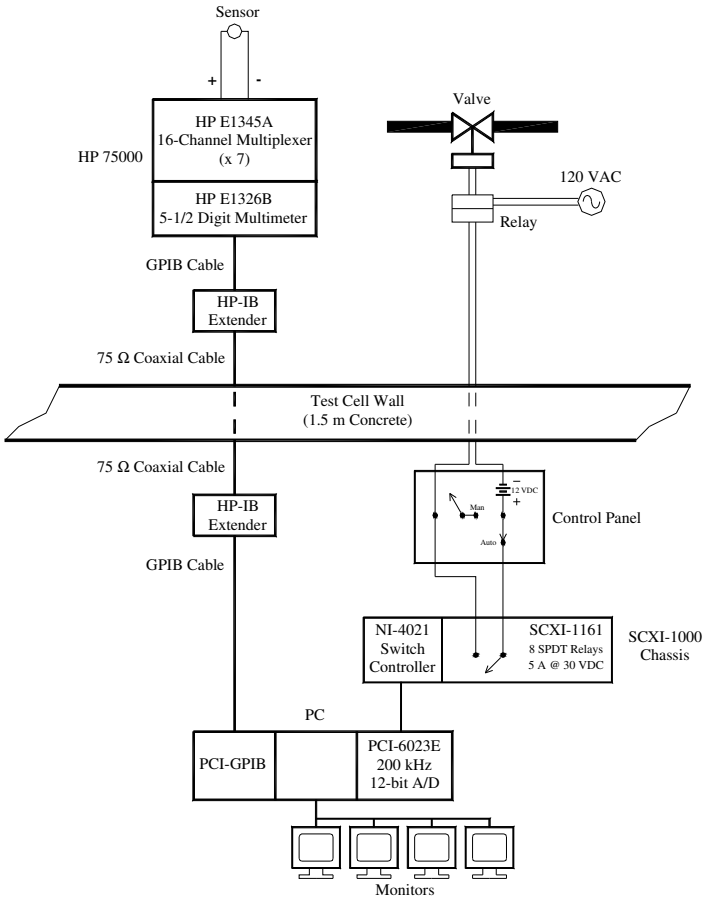

Figure 3.2. Data acquisition and control systems.

Valves are controlled with the PC using a relay card housed within an SCXI chassis (National Instruments). These electromechanical relays are capable of switching up to 8 A at 125 VAC or 5 A at 30 VDC. They are operated via a switch controller in the SCXI chassis, which communicates with the PC through a general-purpose data acquisition card. As shown in Fig. 3.2, the relays in the control room operate devices within the test cell indirectly, through a second relay. This is intended to provide an additional level of electrical isolation between the NI switching hardware and high voltage sources within the cell. As an added safety measure, all wiring is routed through a control panel that can be switched from automatic (PC) control to manual control in the event of computer failure.

4. Test Parameters

The oxide phase of the corium composition for SSWICS-12 will be the same as that of SSWICS-6 [2] (60.3/24.7/15.0 wt % UO_2/ZrO_2/siliceous concrete). The thermite will, however, be slightly reformulated to react at a higher temperature to minimize crust formation on the basemat that might impair initial water flow through the nozzles. The initial melt temperature for SSWICS-6 was ~1950˚C while the target initial temperature for this test is ~2100˚C. The thermite composition for this test is shown in Tables 4.1. Reformulation of the thermite to produce the higher reaction temperature results in a slightly higher Cr metal byproduct content of 7.6 wt % in the melt, which can be compared with to the level of 6.4 wt % for the SSWICS-6 thermite.

Aside from corium composition, the other parameter set that needs to be defined for this test is the individual water heads that are to be applied in each of the four quadrants. In effect, this test can be viewed as a separate effect experiment that is aimed at determining the effect of water head on the local corium quench rate. It was suggested at the 4th PRG meeting that the maximum head should be ~0.2 bar. We have therefore selected heads of 0.05, 0.1, 0.15, and 0.2 bar for the four quadrants.

The proposed test procedure is summarized as follows:

1) Open isolation valves on water lines to nozzles
2) Preheat RV structures to ~100°C (water will not be preheated as in previous tests).
3) Arm thermite ignition system.
4) Ignite thermite to begin test.
5) Note melt peak temperature (usually within one minute of the first sign of ignition).
6) No other operator actions are required until the corium is quenched, which is expected to take place in less than two hours.
7) The melt is considered quenched, and the test complete, when readings from all melt thermocouples reach the saturation temperature of 100°C.

A contingency situation would arise in the event that all of the concrete nozzles failed to open after the thermite burn. This would be evidenced by a lack of thermal loading on the steam condensers that is displayed at the console during the test. In this event, the normal top flooding water injection system will be used to flood the cavity 10 minutes after the burn is completed.

5. References

1. J. Foit, FZK, personal communication to M. T. Farmer, ANL, July 30, 2008.
2. S. Lomperski, M. T. Farmer, D. J. Kilsdonk, and R. W. Aeschlimann, “Small-Scale Water Ingression and Crust Strength Tests (SSWICS); SSWICS-6 Test Data Report: Thermalhydraulic Results,” Rev. 0, OECD/MCCI-2004-TR03, March 19, 2004.

#	Channel	Name	Type	Description	Serial #	Output	Range	Accuracy
0	HPS-0	T-CJ-HPS	AD592 IC	Cold junction compensation sensor.	-	1ξA/K	0-70°C	±0.5°C
1	HPS-1	TM-N-H190	TC type C	Melt temp. 190 mm above bottom of melt (in tungsten thermowell).	-	0-37 mV	0-2320°C	±4.5°C or 1%
2	HPS-2	TM-N-H139	TC type C	Melt temp. 139 mm above bottom of melt (in tungsten thermowell).	-	0-37 mV	0-2320°C	±4.5°C or 1%
3	HPS-3	TM-N-H88	TC type C	Melt temp. 88 mm above bottom of melt (in tungsten thermowell).	-	0-37 mV	0-2320°C	±4.5°C or 1%
4	HPS-4	TM-N-H38	TC type C	Melt temp. 38 mm above bottom of melt (in tungsten thermowell).	-	0-37 mV	0-2320°C	±4.5°C or 1%
5	HPS-5	TM-N-Hm13	TC type C	Melt temp. 13 mm below bottom of melt (in tungsten thermowell).	-	0-37 mV	0-2320°C	±4.5°C or 1%
6	HPS-6	TM-S-H190	TC type C	Melt temp. 190 mm above bottom of melt (in tungsten thermowell).	-	0-37 mV	0-2320°C	±4.5°C or 1%
7	HPS-7	TM-S-H139	TC type C	Melt temp. 139 mm above bottom of melt (in tungsten thermowell).	-	0-37 mV	0-2320°C	±4.5°C or 1%
8	HPS-8	TM-S-H88	TC type C	Melt temp. 88 mm above bottom of melt (in tungsten thermowell).	-	0-37 mV	0-2320°C	±4.5°C or 1%
9	HPS-9	TM-S-H38	TC type C	Melt temp. 38 mm above bottom of melt (in tungsten thermowell).	-	0-37 mV	0-2320°C	±4.5°C or 1%
10	HPS-10	TM-S-Hm13	TC type C	Melt temp. 13 mm below bottom of melt (in tungsten thermowell).	-	0-37 mV	0-2320°C	±4.5°C or 1%
11	HPS-11	TM-E-H190	TC type C	Melt temp. 190 mm above bottom of melt (in tungsten thermowell).	-	0-37 mV	0-2320°C	±4.5°C or 1%
12	HPS-12	TM-E-H139	TC type C	Melt temp. 139 mm above bottom of melt (in tungsten thermowell).	-	0-37 mV	0-2320°C	±4.5°C or 1%
13	HPS-13	TM-E-H88	TC type C	Melt temp. 88 mm above bottom of melt (in tungsten thermowell).	-	0-37 mV	0-2320°C	±4.5°C or 1%
14	HPS-14	TM-E-H38	TC type C	Melt temp. 38 mm above bottom of melt (in tungsten thermowell).	-	0-37 mV	0-2320°C	±4.5°C or 1%
15	HPS-15	TM-E-Hm13	TC type C	Melt temp. 13 mm below bottom of melt (in tungsten thermowell).	-	0-37 mV	0-2320°C	±4.5°C or 1%
16	HPS-16	TM-W-H190	TC type C	Melt temp. 190 mm above bottom of melt (in tungsten thermowell).	-	0-37 mV	0-2320°C	±4.5°C or 1%
17	HPS-17	TM-W-H139	TC type C	Melt temp. 139 mm above bottom of melt (in tungsten thermowell).	-	0-37 mV	0-2320°C	±4.5°C or 1%
18	HPS-18	TM-W-H88	TC type C	Melt temp. 88 mm above bottom of melt (in tungsten thermowell).	-	0-37 mV	0-2320°C	±4.5°C or 1%
19	HPS-19	TM-W-H38	TC type C	Melt temp. 38 mm above bottom of melt (in tungsten thermowell).	-	0-50 mV	0-1250°C	±2.2°C or 0.75%
20	HPS-20	TM-W-Hm13	TC type C	Melt temp. 13 mm below bottom of melt (in tungsten thermowell).	-	0-50 mV	0-1250°C	±2.2°C or 0.75%
21	HPS-21	TG-RV	TC type C	Gas temp. in reaction vessel upper plenum.	-	0-50 mV	0-1250°C	±2.2°C or 0.75%
22	HPS-22	TS-RV-tf	TC type K	Temperature of RV top flange.	-	0-50 mV	0-1250°C	±2.2°C or 0.75%
23	HPS-23	TS-RV-1000	TC type K	Outer wall temp. of RV 1000 mm above bottom of melt.	-	0-50 mV	0-1250°C	±2.2°C or 0.75%
24	HPS-24	TS-RV-mf	TC type K	Temperature of RV middle flange.	-	0-50 mV	0-1250°C	±2.2°C or 0.75%
25	HPS-25	TS-RV-100	TC type K	Outer wall temp. of RV 100 mm above bottom of melt.	-	0-50 mV	0-1250°C	±2.2°C or 0.75%
26	HPS-26	TS-RV-bf	TC type K	Temperature of RV bottom flange.	-	0-50 mV	0-1250°C	±2.2°C or 0.75%
27	HPS-27	TS-vent	TC type E	Outer wall temp. of vent line.	-	0-70 mV	0-900°C	±1.7°C or 0.5%
28	HPS-28	TF-CT-102	TC type K	Fluid temp. in condensate tank at a water level of 102 mm.	-	0-50 mV	0-1250°C	±2.2°C or 0.75%
29	HPS-29	TF-CT-406	TC type K	Fluid temp. in condensate tank at a water level of 406 mm.	-	0-50 mV	0-1250°C	±2.2°C or 0.75%
30	HPS-30	TF-CT-711	TC type K	Fluid temp. in condensate tank at a water level of 711 mm.	-	0-50 mV	0-1250°C	±2.2°C or 0.75%
31	HPS-31	TF-CT-1016	TC type K	Fluid temp. in condensate tank at a water level of 1016 mm.	-	0-50 mV	0-1250°C	±2.2°C or 0.75%
32	HPS-32	TF-CT-1321	TC type K	Fluid temp. in condensate tank at a water level of 1321 mm.	-	0-50 mV	0-1250°C	±2.2°C or 0.75%
33	HPS-33	TF-CT-1626	TC type K	Fluid temp. in condensate tank at a water level of 1626 mm.	-	0-50 mV	0-1250°C	±2.2°C or 0.75%
34	HPS-34	TF-HX-in	TC type K	Fluid temp. at HX coolant inlet.	-	0-50 mV	0-1250°C	±2.2°C or 0.75%
35	HPS-35	TF-HX-out	TC type K	Fluid temp. at HX coolant outlet.	-	0-50 mV	0-1250°C	±2.2°C or 0.75%

Table 3.1. Instrumentation list for water ingression tests (part 1 of 2).

36	HPS-36	HF-vent	Thermopile	Heat Flux through connecting line to V-ST.	0632	0-5.50 mV	0-5 kW/m^2	±3%
37	HPS-37	I-ign	DC supply	Current supply for thermite ignitor.	-	0-100 mV	0-25 Amps	-
38	HPS-38	TF-quench	TC type K	Temperature of water injected into RV	-	0-50 mV	0-1250°C	±2.2^{o}C or 0.75%
39	HPS-39	Reserve	-	-	-	-	-	-
40	HPS-40	PA-RV	1810AZ	Absolute pressure in reaction vessel.	02351-00P1PM	1-6 V	0-14 bar gage	±0.14 bar
41	HPS-41	PD-CT	1801DZ	ξP transmitter to measure condensate inventory.	-	0-13 V	0-0.35 bar	±0.004 bar
42	HPS-42	L-TDR-CT	BM100A	Time domain reflectometer to measure CT level.	A02331879A	4 - 20 mA	0 - 2 m	±3 mm
43	HPS-43	VDC-P-supply	-	Voltage of the power supply for the pressure transmitters.	-	0 - 15 V	-	-
44	HPS-44	Reserve	-	-	-	0 - 5 V	0-50 sl/m Ar	±0.5 sl/m
45	HPS-45	Reserve	-	-	-	0-37 mV	0-2320°C	±4.5^{o}C or 1%
46	HPS-46	Reserve	-	-	-	0-37 mV	0-2320°C	±4.5^{o}C or 1%
47	HPS-47	Reserve	-	-	-	0-37 mV	0-2320°C	±4.5^{o}C or 1%
48	HPS-48	Reserve	-	-	-	0-37 mV	0-2320°C	±4.5^{o}C or 1%
49	HPS-49	Reserve	-	-	-	0-37 mV	0-2320°C	±4.5^{o}C or 1%
50	HPS-50	Reserve	-	-	-	0-37 mV	0-2320°C	±4.5^{o}C or 1%
51	HPS-51	PD-R05	-	ξP transmitter to measure level in reservoir with 0.5 m head.	-	0-13 V	0-0.35 bar	±0.004 bar
52	HPS-52	PD-R1	-	ξP transmitter to measure level in reservoir with 1.0 m head.	-	0-13 V	0-0.35 bar	±0.004 bar
53	HPS-53	PD-R15	-	ξP transmitter to measure level in reservoir with 1.5 m head.	-	0-13 V	0-0.35 bar	±0.004 bar
54	HPS-54	PD-R2	-	ξP transmitter to measure level in reservoir with 2.0 m head.	-	0-13 V	0-0.35 bar	±0.004 bar
55	HPS-55	Reserve	-	-	-	-	-	-
56	HPS-56	Reserve	-	-	-	-	-	-
57	HPS-57	Reserve	-	-	-	-	-	-
58	HPS-58	Reserve	-	-	-	-	-	-
59	HPS-59	Reserve	-	-	-	-	-	-
60	HPQ-50	T-CJ-HPQ	AD592 IC	Cold junction compensation sensor.	-	1ξA/K	0-70°C	±0.5^{o}C
61	HPQ-51	TF-ST	TC type K	Fluid temp. in spray tank.	-	0-50 mV	0-1250°C	±2.2^{o}C or 0.75%
62	HPQ-52	TG-CL-out	TC type K	Gas temperature in condensate tank outlet line to spray tank.	-	0-50 mV	0-1250°C	±2.2^{o}C or 0.75%
63	HPQ-53	TG-ST-in	TC type K	Gas temp. in the spray tank line inlet.	-	0-50 mV	0-1250°C	±2.2^{o}C or 0.75%
64	HPQ-54	TG-ST-out	TC type K	Gas temp. in the spray tank line outlet.	-	0-50 mV	0-1250°C	±2.2^{o}C or 0.75%
65	HPQ-55	F-quench	Paddlewheel	Flow rate of water into reaction vessel (for quenching melt).	3144	0-5 V	0-50 gpm	±0.5 gpm
66	HPQ-56	F-HX	Paddlewheel	Flow rate of cold water to heat exchangers.	3143	0-5 V	0-50 gpm	±0.5 gpm

Table 3.1. (continued).

LabVIEW Channel #	Valve Name	Description	Actuator
1	V-CT	Valve on steam line between reaction vessel and quench tank.	Pneumatic
2	V-quench	Valve on quench water supply line into reaction vessel.	Solenoid
3	V-quench-i	Isolation valve on quench water supply line into reaction vessel.	Solenoid
4	V-quench-b	Valve on back-up quench water supply.	Solenoid
5	V-ST	Valve on vent line between reaction vessel and spray tank.	Pneumatic
Panel	V-HX	Valve on cooling-water line to heat exchangers.	Solenoid
Panel	VC-CT	Control valve on steam line between reaction vessel and quench tank.	Electric

Table 3.2. Remotely operated valves.

Constituent	Mass (kg)
U_3O_8	78.61
CrO_3	19.90
CaO	2.96
Zr	22.98
Mg	0.10
Si	3.51
SiO_2	7.49
Al	0.45
Total	136.0

Constituent	Wt %	
	Reactant	Product
U_3O_8	57.80	-
UO_2	-	55.61
Zr	16.90	-
ZrO_2	-	22.84
Si	2.58	-
SiO_2	5.51	11.03
Mg	0.07	-
MgO	-	0.11
Al	0.33	-
Al_2O_3	-	0.63
CaO	2.18	2.18
CrO_3	14.63	-
Cr	-	7.60

Tables 4.1. Corium powder charge and reaction product mass fractions.

Appendix A: Thermite and Nozzle Scoping Tests

The concrete nozzles that are used to inject water into the bottom of the melt for SSWICS-12 represent a new design feature for the Category 2 tests. Since these items are not commercially available, developmental tests were carried out with the objectives to: i) gain experience in the manufacturer of these items, ii) characterize their permeability, and iii) verify that the specific nozzle design developed for SSWICS-12 will open upon contact with melt so that the follow-on debris quenching behavior can be characterized. This appendix documents the various activities that were carried out to meet these objectives.

The first step in this process was to carry out 'nozzle scoping tests' that included fabricating several test nozzles and then performing water permeability tests in order to characterize pressure drop across the porous concrete and to check that the concrete maintained structural integrity as the water passed through the porous media. With this step completed, a 'nozzle thermite test' was carried out to verify that the nozzles would open upon contact with the corium shortly after the thermite burn is completed. The results are presented for these two stages of testing below.

A.1 Nozzle Scoping Tests

A few benchtop tests were first performed in order to characterize flow behavior through the concrete nozzles and to verify structural stability of the concrete media. A total of six nozzles were fabricated for testing (Figure A.1). The first two were used for shakedown testing of the simple apparatus that was developed to mock up conditions expected for SSWICS-12. The other 4 were used for quantitative testing after the apparatus (Figure A.2) was perfected. The apparatus simply consisted of a reservoir fixed at an elevation above the top of the nozzle. The reservoir had a capacity of 2.44 liters of water and was open to the atmosphere at the top. The initial water height (head) above the top of the nozzles was 123 cm. After the 2.44 liters of water volume had drained from the reservoir, the head was reduced to 108 cm. Thus, the effective water head on the nozzles varied from about 12.1 kPa at the start of the transient to 10.6 kPa at the end. The diameter of the connecting tube was selected to be large (1.9 cm) so that the tubing would not offer a significant flow resistance in the system.

The results for the various tests that were conducted to characterize the system setup and the nozzle flow behavior are shown in Table A.1. As is evident, the flowrate through the system with the tubing alone was large; i.e., 14.6 l/min. For comparison, if one selects a design quench rate of 1 MW/m^2 for SSWICS-12, then the total basemat water injection flowrate would need to be ~ 1.63 l/minute (assuming room temperature water) to provide this amount of coolant, or ~ 0.41 l/minute to each of the four quadrants. The flowrate through the system in an unimpeded state was thus an order of magnitude greater than this total water injection rate.

Test No.	Orifice Size (mm)	Concrete Nozzle No.	Δt for water level change from 2.44 l → 0 (sec)	Average flowrate (liters/minute)
1	None	None	10	14.6
2	2	None	177	0.83
3	None	2	63	2.32
4	2	3	198±6	0.74
5	2	4	208±2	0.71
6	2	5	187±3	0.78
7	2	6	191±2	0.77

Table A.1. Benchtop test results.

Figure A.1. Nozzle preparation.

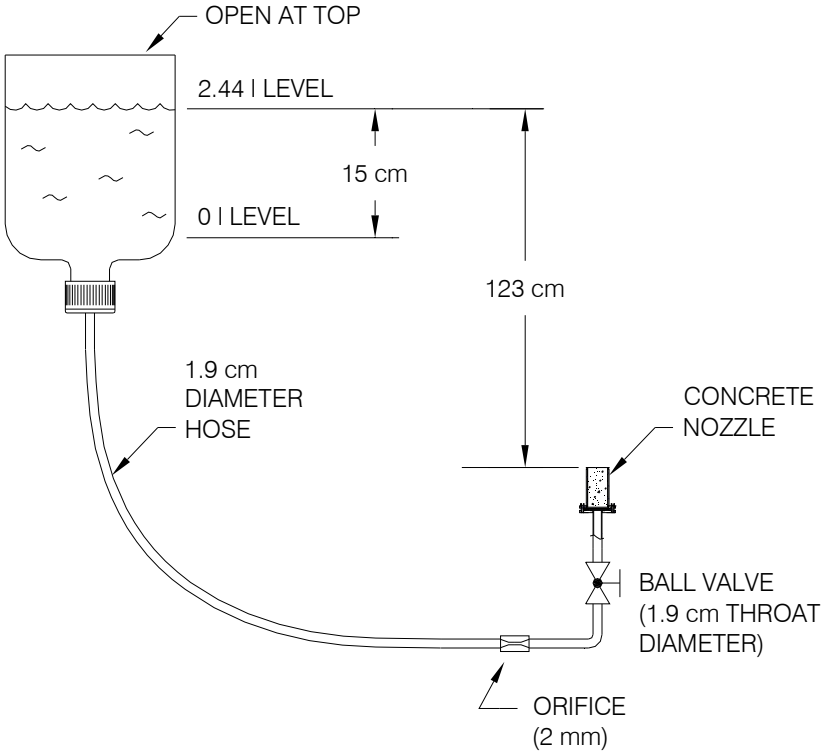

Figure A.2. Benchtop experimental setup.

Based on design calculations, an orifice diameter of 2 mm was sized to provide ~ 0.4 l/minute to a concrete nozzle (assuming no significant pressure drop across the nozzle). This nozzle was then tested three times to measure flowrate; times varied from 176-178 seconds, and based on an average of 177 seconds, the actual flowrate was ~ 0.83 l/minute which is about a factor of 2 above the rate required to quench the debris at a rate of 1 MW/m^2. In any case, the 2 mm orifice was used for further testing of the concrete nozzles.

Subsequently, one nozzle was tested without an orifice to characterize pressure drop across the porous concrete. The flowrate was found to be 2.32 l/minute, which is about a factor of 6 above the design level of 0.4 l/minute. Thus, the conclusion was drawn that the pressure drop across the porous media is not large at the design flowrate, and so the flow can be adequately controlled using only the pressure drop across the orifice (as opposed to the more complicated situation in which the pressure drop across the porous media would need to be included in the flowrate reduction calculation).

Thereafter, the remaining 4 sample nozzles were tested to determine flow behavior. As shown in the table, the average flowrate results clustered quite close to 0.75 l/minute. All tests were repeated twice, so a total of about 4.9 liters of water was passed through each nozzle. The time ranges shown reflect the variations in drainages times observed in the repeat tests.

In terms of phenomenology, in all nozzle tests the water flow through the specimens was found to rinse out the mortar. In particular, the water seen flowing through the specimens was grayish for the first 15-20 seconds of the transients, at which point the water ran clear. At this point, the aggregate was clearly evident in its original, natural state.

The material left in the nozzles at the end of the test was essentially gravel, and a small amount would fall out when the specimens were removed from the test stand. As noted earlier, all tests were repeated twice, and the gravel stayed pretty much in place over these tests. Also, the drainage rate (permeability) did not change much over the course of the two tests. On this basis, it probably does not matter that the mortar washes out, and the specimens will most likely perform well when used in the quenching test.

A.2 Nozzle Thermite Test

Based on the results of the nozzle scoping tests, a nozzle thermite test was carried out to characterize the performance of the nozzles under prototypic conditions in which the melt would come into direct contact with the tops of these units after the thermite burn was completed. This test also offered the opportunity to check thermite reaction temperature and melt fluidity upon reaction for the new thermite that was designed for this experiment. Thus, the specific goals of this test were to: i) verify nozzle opening upon contact with corium following the thermite reaction, and ii) evaluate the reaction temperature and burn characteristics for the thermite to be used in the full scale test.

A schematic of the overall system setup is shown in Figure A.3, while details of the reaction cup are shown in Figure A.4. A photograph of the actual setup inside the test drum is provided in Figure A.5. The thermite was contained within an MgO test crucible. The crucible was fitted with two Type C thermocouples to measure thermite reaction temperature. The crucible was also modified so that a sample nozzle could be installed within, thereby mocking up the conditions within the test section. The space around the nozzle was filled with silica sand so that the nozzle was essentially flush with the sand surface. The nozzle was connected to a gas bottle so that a gas pressure of ~ 10 kPad could be applied to mock up a typical water head applied to the nozzles during the full scale test. The line also contained a differential pressure transducer to detect the time at which the nozzle opened (by virtue of a drop in gas pressure)

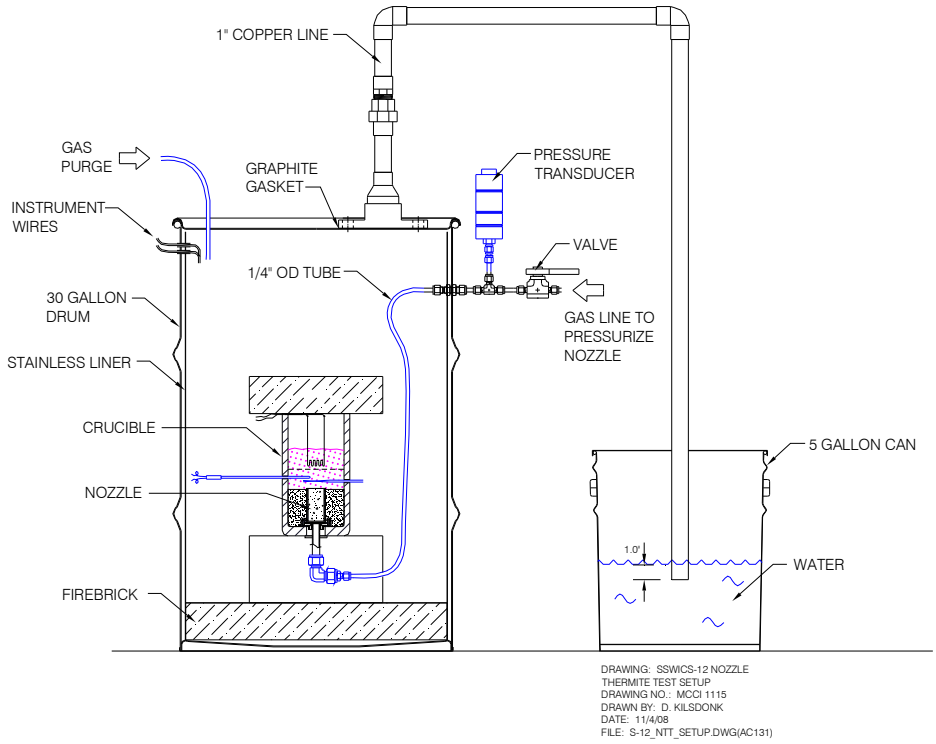

Figure A.3. Overall system setup.

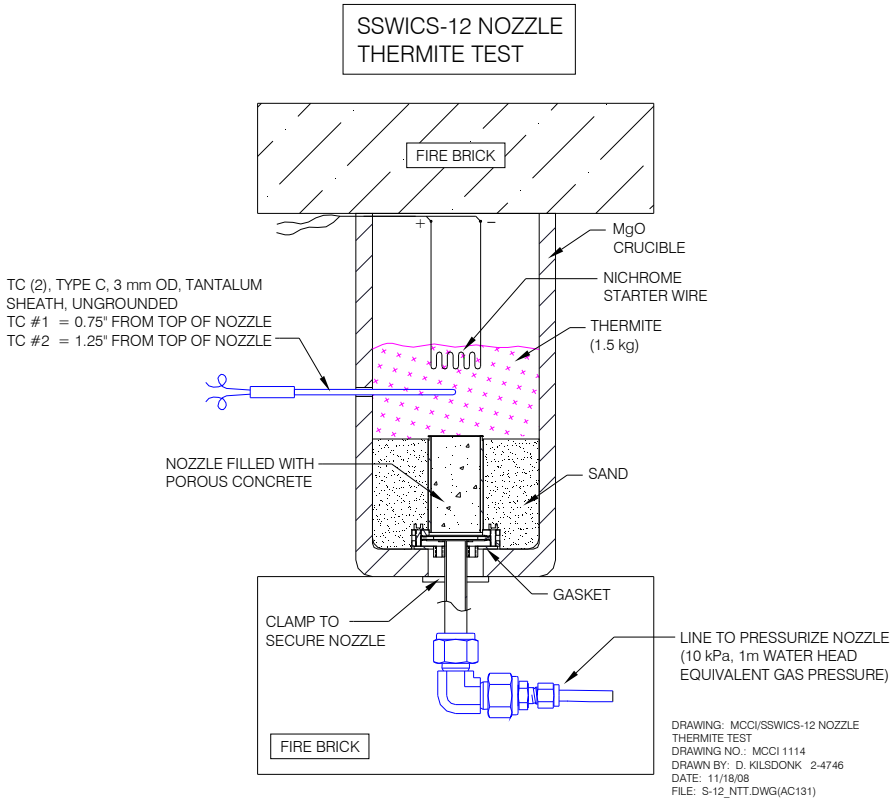

Figure A.4. Details of reaction crucible setup.

Figure A.5. Top view of assembly before thermite loading.

following contact by the corium. The composition of the thermite charge (Table A.2) was identical to that planned for the full scale test. A firebrick was placed on top of the crucible to prevent melt splatter within the test drum during the burn. Finally, a nichrome heater wire was used to ignite the thermite near the top of the charge.

The experiment procedure was as follows. After the system was setup as shown in Figures A.3 and A.4, the drum was inerted with a slow argon purge for several hours. A gas pressure of ~ 10 kPad was then applied to the line leading to the nozzle inlet, and after target pressure was reached the line was closed to create a sealed system. The thermite was then ignited and the system response was recorded on a data acquisition system. The materials were then allowed to cool overnight before removal and examination to characterize the posttest debris configuration.

A plot showing the melt temperature and nozzle pressure response is provided in Figure A.6. As is evident, the gas pressure inside the nozzle increased slightly as the burn progressed; this is due to heatup of the gas inside the closed nozzle. As is evident, the nozzle opened almost immediately upon contact by the melt, as evidenced by the sudden reduction in gas pressure system at 61 seconds. The recorded reaction temperature for this thermite was ~ 2100 ºC, which is ~ 150 ºC higher than that recorded for the SSWICS-6. Thus, this test verified: i) an increase in the thermite reaction temperature, and ii) rapid opening of the basemat nozzle upon melt contact.

Constituent	Reactant Wt %	Mass (g)
U_3O_8	57.95	869.25
Zr	16.94	254.1
Si	2.58	38.7
SiO_2	5.52	82.8
CaO	2.18	32.7
Mg	0.07	1.05
Al	0.08	1.20
CrO_3	14.68	220.2
Total/Average	100.0	1500

Table A.2. Thermite charge for nozzle test.

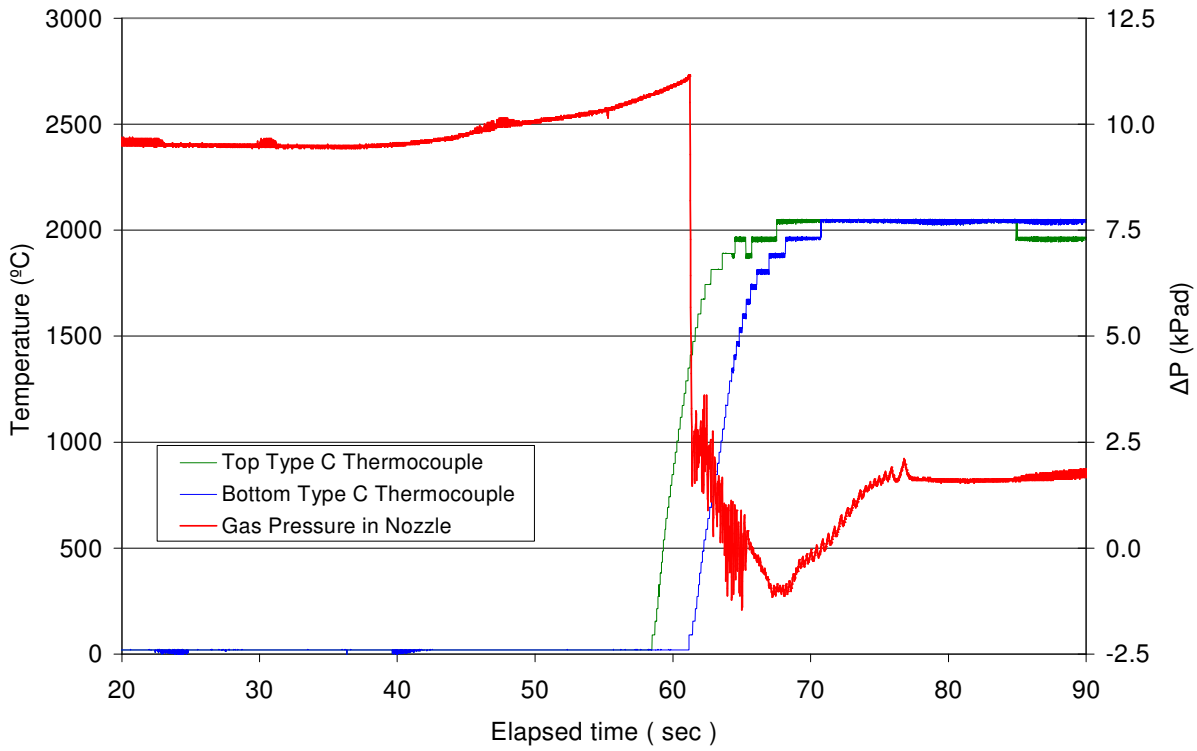

Figure A.6. Reaction temperature and nozzle pressure for thermite test

Photographs showing the test assembly during various stages of disassembly are provided in Figures A.7 through A.9, while an additional picture of the test nozzle after removal is provided in Figure A.10. A thin film of solidified corium was deposited on the sides of the crucible as well as on the underside of the firebrick during the burn. The powders packed to within ~ 2.5 cm of the top of the crucible, and so this film was deposited as the burn progressed and the melt slumped into a pool with very low porosity. The thinness of the sidewall crust material as well as the density of the material remaining over the nozzle indicates that this corium composition was quite fluid upon reaction. As shown in Figure A.10, the nozzle survived the experiment in quite good shape; some of the aggregate came out during removal but this was due to the fact that the uppermost material had bonded to the corium.

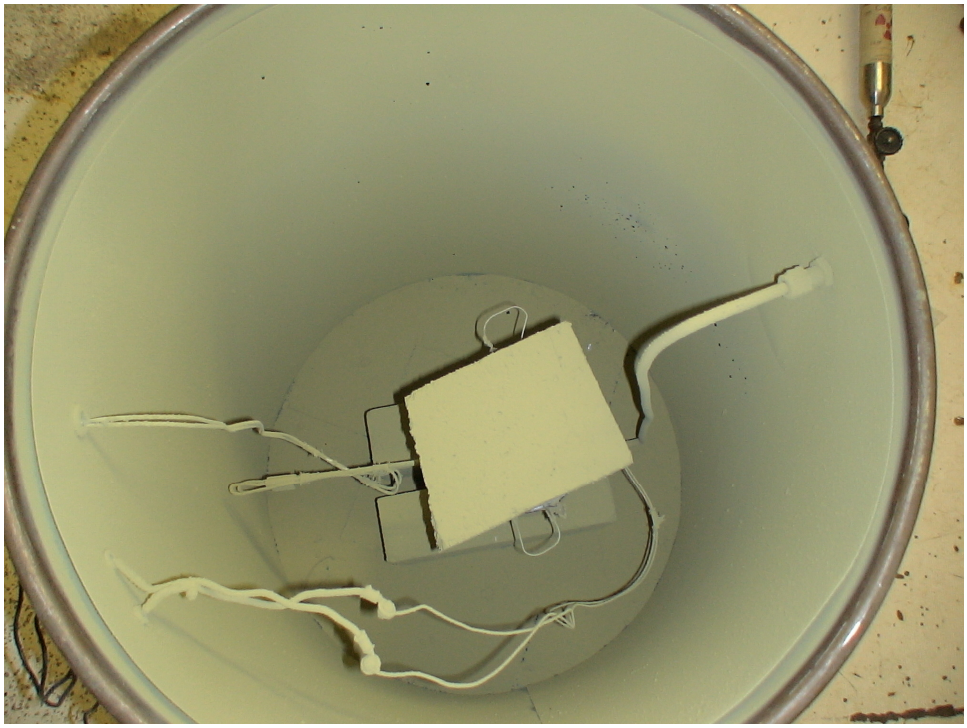

Figure A.7. Top view assembly two days after the experiment

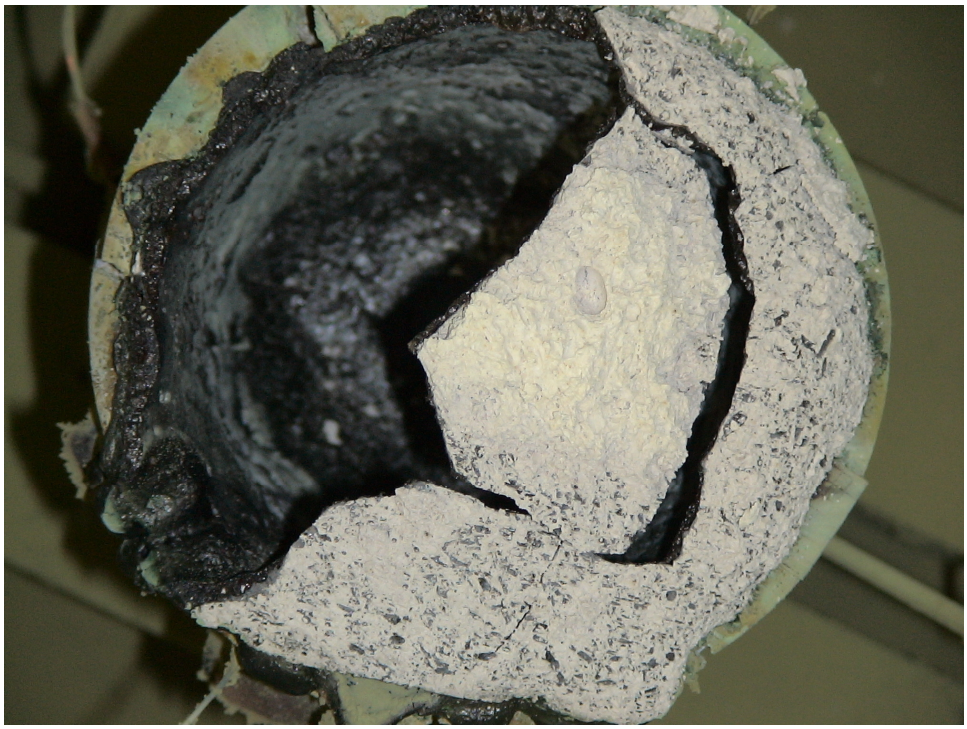

Figure A.8. Melt product and fire brick residue on top of the MgO cylinder.

Figure A.9. The cavity after removing the solidified corium.

Figure A.10. The nozzle after the test.